Petrogenesis of the Railroad Mountain Alkali Olivine Diabase Dike: Intrusion at the Edge of the Stable Craton in Eastern New Mexico

James Constantopoulos[1]

[1] Department of Physical Sciences, Eastern New Mexico University, Portales, NM 88130; Jim.Constantopoulos@enmu.edu

https://doi.org/10.58799/NMG-v46n1.1

Abstract

The Railroad Mountain dike is a single-phase alkali olivine diabase intrusion located in east-central New Mexico that represents the easternmost igneous body in the Lincoln County porphyry belt, which is part of the post-Laramide Rocky Mountain alkalic province. The dike forms a resistant ridge, Railroad Mountain, approximately 50 km long, 30–45 m wide, and up to 25 m high. Two new groundmass $^{40}Ar/^{39}Ar$ ages are nearly identical, averaging 27.66 ± 0.03 Ma. The dike rocks are uniformly fine-grained and unaltered except for minor local effects, with textures in thin sections ranging from fine-grained trachytic to diabasic. Modal mineralogy averages 60% plagioclase, 20% augite, 10% olivine, 10% opaques (magnetite and ilmenite), and accessory apatite. Major element oxide concentrations from 37 samples are remarkably consistent, with differences between minimum and maximum concentrations of less than 1 wt% for all oxides. The mean silica concentration is 47.51 ± 0.18 wt%, the MgO concentration is 5.05 ± 0.071 wt%, and Na_2O is greater than K_2O. Mg#s average 41.84 ± 0.43, and the concentrations of TiO_2, FeO*, CaO, and Sc increase with decreasing Mg#, suggesting clinopyroxene fractionation. The decrease in Cr and Ni with decreasing Mg# likely reflects changes in olivine composition during differentiation. The silica and alkali values plot in a tight cluster in the trachybasalt field on the total alkali-silica diagram and are nepheline normative. Geochemically, the rocks are classified as sodic alkali trachybasalts. The light rare earth elements (LREEs) are moderately enriched (La/Yb_N = 12.72–13.26), with minimal heavy rare earth element (HREE) enrichment (Tb/Yb_N = 2.37–2.48) and negligible Eu anomalies (Eu/Eu* = 0.94–0.98). The lack of HREE fractionation indicates an asthenospheric mantle source with no residual garnet. The large ion lithophile elements (LILEs) are enriched 26 to 160 times primitive mantle values, and the high field strength elements (HFSEs) are enriched 14 to 98 times primitive mantle values. All samples plot in the within-plate field on the tectonic discrimination diagram. Microprobe analyses on two thin sections yielded an average olivine composition of $Fo_{49.0}Fa_{49.8}Tp_{1.2}$ and an average clinopyroxene composition of $Wo_{43.1}En_{38.4}Fs_{16.7}Ac_{1.7}$. Magnetite-ilmenite geothermometer temperatures and oxygen fugacity calculations yielded an average temperature of 1209°C and $\mathrm{Log}_{10} fO_2$ = -7.31. Petrogenetic modeling was done using spinel lherzolite REE chemistry and Kilbourne Hole mineralogy as a source. The results of nonmodal equilibrium and nonmodal fractional batch melting models are similar and indicate a small degree (~5%) of partial melting of a spinel lherzolite source. The dike intruded at the edge of the stable North American craton during the post-Laramide foundering and tearing of the Farallon slab that had previously metasomatized the lithosphere. This process intensified asthenospheric upwelling, resulting in melting and intrusion of the dike just prior to or coeval with the initiation of Rio Grande rifting.

Introduction

Eocene–Oligocene igneous rocks of the Lincoln County porphyry belt (LCPB; Fig. 1) are part of the post-Laramide Rocky Mountain alkalic province that extends along the eastern front of the Rocky Mountains from Canada to Mexico (Carmichael et al., 1974; Mutschler et al., 1985, 1991; Woolley, 1987; McLemore, 1996). Igneous activity occurred along the boundary between the stable craton to the east and rocks deformed during the Laramide orogeny to the west, with magmatism taking place during the protracted transition between Laramide contraction and subsequent extension (Allen and Foord, 1991). The edge of the stable craton in this part of New Mexico is represented by relatively undeformed Paleozoic and Mesozoic strata of the Pecos slope (Kelley, 1971; Allen and McLemore, 1991).

Allen and Foord (1991) identified two periods of igneous activity in the LCPB. The first was late Eocene (38.2–36.5 Ma) and was concentrated along the Pedernal arch, where alkali gabbro to syenite and equivalent volcanic rocks of the Sierra Blanca igneous complex were emplaced along subordinate northeast-trending faults. This occurred during the transition from Laramide compression to extension. The second period was in the Oligocene (30.0–26.5 Ma), during which mafic alkalic dikes and granite plutons were emplaced along the Capitan lineament and syenite, minor granite, and rhyolite were intruded 29.0–25.4 Ma into the Sierra Blanca complex (Goff et al., 2014). This later period is associated with the early stages of Rio Grande rifting. Igneous activity continued with the eruption of the Holocene Carrizozo basalt flows in the western portion of the LCPB at 5 ka.

Major dikes extending out from the center of the LCPB, including the Railroad Mountain and Jones Camp dikes (Fig. 1), represent near snapshots in time of deformation, magmatic systems, and the lithosphere at a key junction between the active cordillera and stable interior during a profound tectonic transition. The Railroad Mountain dike, the easternmost igneous body in the LCPB (Fig. 1), is a single-phase mafic intrusion located on the Mescalero pediment, east of the Pecos River in Chaves County, New Mexico. Several smaller dikes lie to the south, and all are probably related (Semmes, 1920).

This work combines new mineralogical, geochemical, and geochronological data as well as petrogenetic interpretations to characterize the Railroad Mountain dike. This study adds to our understanding of late Cenozoic magmatism on the High Plains adjacent to the Rio Grande rift. A second objective is to use the mineralogical and geochemical information to develop a petrogenetic model. The final objective is to place the formation of the dike in the context of the subducting Farallon slab and the transition between the Laramide orogeny and the initiation of Rio Grande rifting.

Geologic Setting

The Railroad Mountain dike and smaller associated dikes lie east of the Pecos River just west of the Llano Estacado that bounds the High Plains. The dike was first mentioned by Fisher (1906) and Semmes (1920). Allen and Foord (1991) provided some preliminary data in their work on the Lincoln County porphyry belt. These intrusions lie along the west-northwest-trending Capitan lineament, which extends from the Matador arch in west Texas westward toward Socorro, New Mexico, and possibly even farther west (Allen and Foord, 1991; Cather, 1991; Bartsch-Winkler, 1992). The lineament is defined by structural (Ewing, 1990) and magmatic features (Kelley, 1971) and is considered a leaky transverse fracture of the Rio Grande rift or a "basement flaw" (Chapin et al., 1978). Aldrich et al. (1986) reported a single K-Ar date of 27.9 ± 1.4 Ma.

The Railroad Mountain dike forms a resistant ridge (Fig. 2) approximately 50 km long, 30–45 m wide, and up to 25 m high (Semmes, 1920; Kelley, 1971; Allen and Foord, 1991; Bartsch-Winkler, 1992). Because competent aggregate resources are rare in this part of New Mexico, Railroad Mountain and adjacent dikes have been periodically quarried for road metal since the 1960s (Bartsch-Winkler, 1992). Along most of its length, the dike is partially covered by the eolian Mescalero sands (Quaternary) and is in local contact with the Late Triassic Chinle Group in the eastern half and the Triassic Santa Rosa Sandstone and rocks of the Permian Artesia Group at the far western end (Fig. 3). The eastern extension is buried under the Mescalero sands, with the

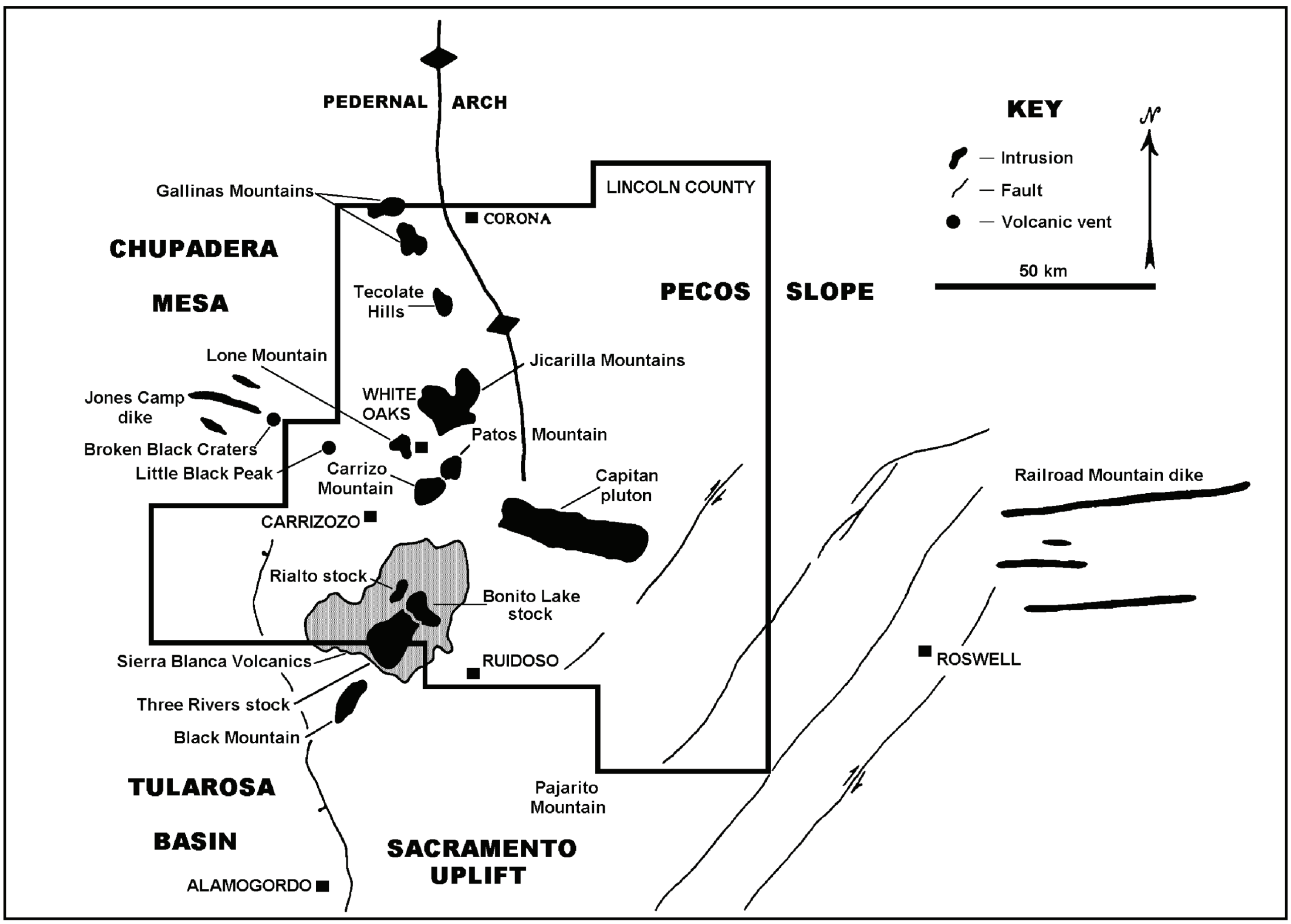

Figure 1. The Lincoln County porphyry belt and other regional features. The Capitan lineament includes Railroad Mountain, the Capitan pluton, and the Jones Camp dike to the west. The Sierra Blanca igneous complex includes the Sierra Blanca volcanics and associated stocks. The edge of the stable craton is manifested by the relatively undeformed Paleozoic and Mesozoic Pecos slope (Allen and McLemore, 1991). From Constantopoulos (2007), modified after Allen and Foord (1991).

Figure 2. Railroad Mountain dike in the area of greatest relief. View is looking to the north.

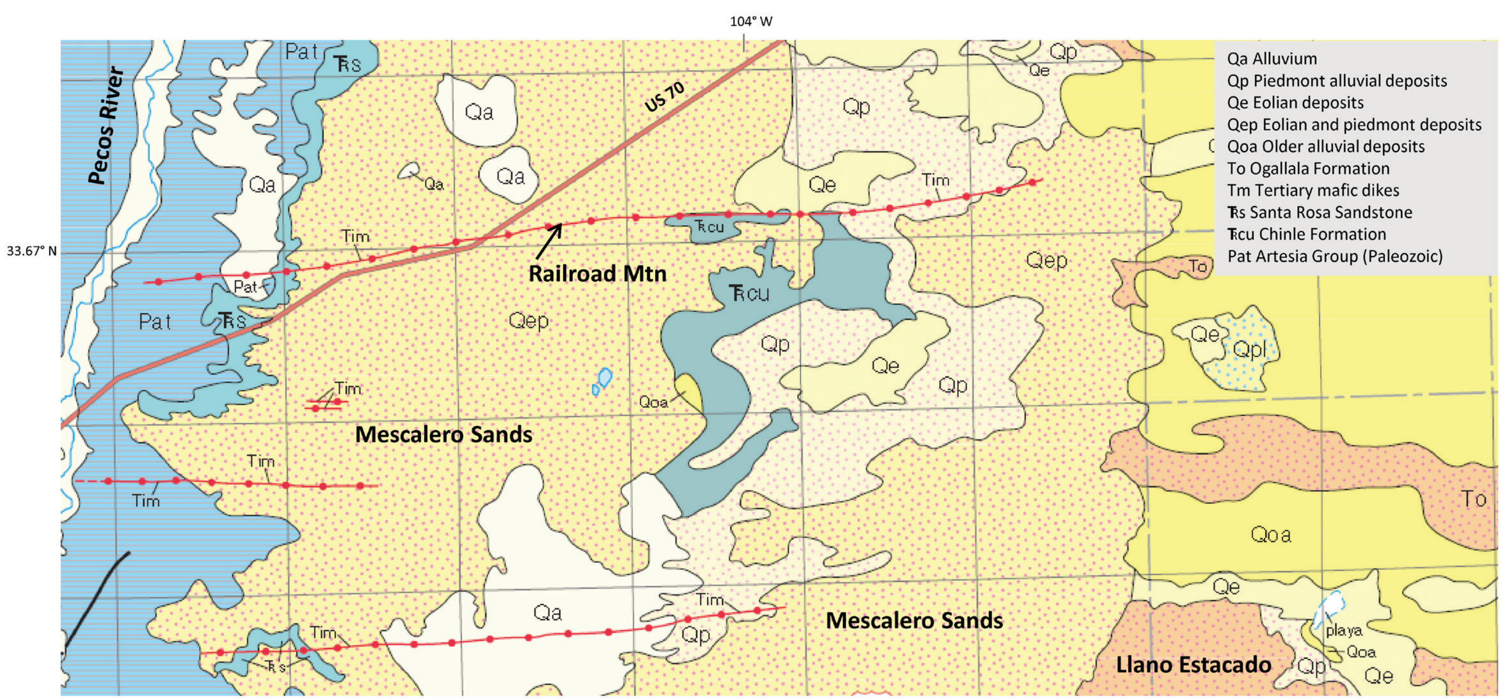

Figure 3. Geologic map showing the location of the Railroad Mountain dike (red dotted line) and related features. The region east of the Pecos River is referred to as the Mescalero pediment of the Pecos slope (see Fig. 1). Adapted from NMBGMR (2003).

distal end not exposed; the western end is lost under river deposits east of the Pecos River and is not exposed west of the Pecos River (Semmes, 1920). From east to west, the trend of the dike changes from east-northeast to west-southwest, which is in line with Capitan Mountain, located to the west. Contact metamorphic effects are minimal, and there is typically only a minor bake zone. In a borrow pit located near the center of the exposed portion of the dike, the sharp contact between the dike and the Chinle Group is well displayed along the southern wall of the pit (Fig. 4). Along the northern wall of the pit, shearing of the country rock and prominent jointing of the dike are well exposed (Fig. 5). Some dike samples along the contacts contain small vugs that contain clays and minor calcite, yielding a spotted appearance (Fig. 6).

Methods

For this study, two samples were submitted to the New Mexico Bureau of Geology and Mineral Resources for groundmass whole rock $^{40}Ar/^{39}Ar$ age determinations (New Mexico Geochronology Research Laboratory [https://geoinfo.nmt.edu/labs/argon/]). The ages for the two samples were nearly identical and averaged 27.66 ± 0.03 Ma. The age spectra are shown in Figure 7.

Samples for geochemical and thin-section analyses were collected along the dike over a distance spanning approximately 16 km (Fig. 8). Beyond this distance, the dike is poorly exposed or weathered. Several samples were collected from the walls of quarries to investigate vertical changes. Mineralogy and textures were described from petrographic thin sections.

Figure 4. Sharp contact between the Railroad Mountain dike (dark color) and sandstone of the Chinle Formation (tan-brown) along the southern wall of a quarry located near the center of the exposed portion of the dike. Note the color change of the diabase at the contact in the top photo.

Figure 5. Shearing (top) and jointing (bottom) at the contact along the northern wall of a quarry located near the center of the exposed portion of the dike. The horizontal view is approximately 2.5 m in both photos.

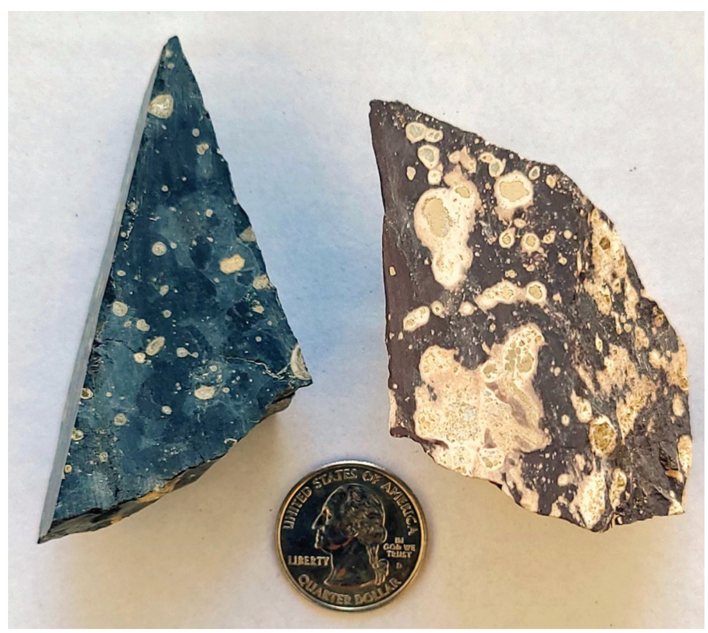

Figure 6. Photograph of hand samples (left: RRM-23, right: RRM-8) from the contact zone that reacted with the county rock. The small vugs are filled with clay and calcite. The sample on the right is heavily oxidized, resulting from a stronger reaction with the country rock.

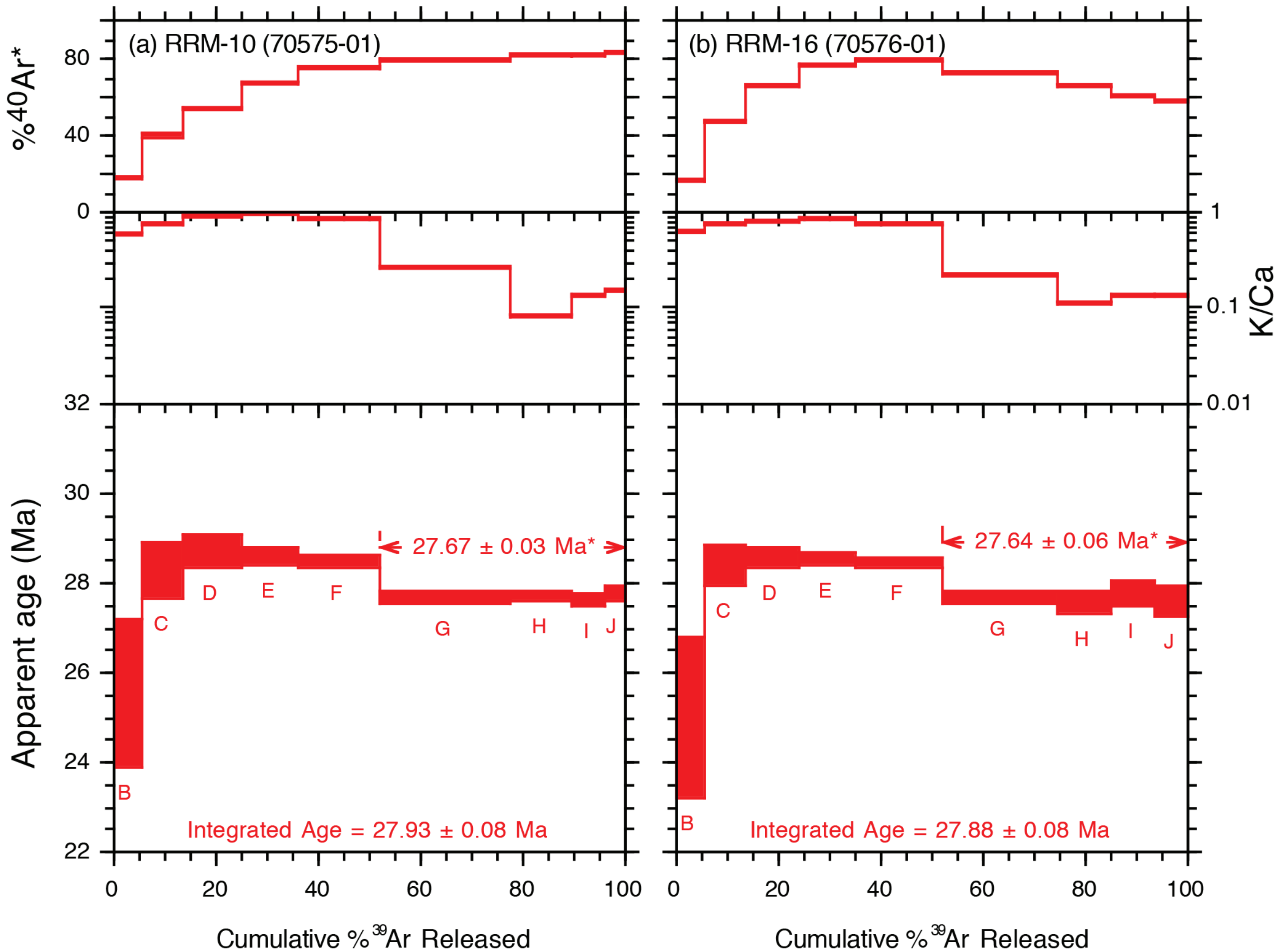

Figure 7. $^{40}Ar/^{39}Ar$ groundmass age spectra of samples RRM-10 and RRM-16. The average age is 27.66 ± 0.03 Ma. Dating of the samples was provided by the New Mexico Bureau of Geology and Mineral Resources.

Figure 8. Railroad Mountain sample locations. Some symbols represent locations where several closely spaced samples were collected. The quarry samples were collected along the north and south walls of a quarry spaced over a horizontal distance of approximately 30 m. Google Earth image dated 6/14/2023.

Forty samples were analyzed by X-ray fluorescence and inductively coupled plasma mass spectrometry for major, minor, and trace elements by the Peter Hooper GeoAnalytical Laboratory at Washington State University (Table 1[1]). See Johnson et al. (1999) and https://environment.wsu.edu/facilities/geoanalytical-lab/ for a discussion of procedures and techniques. Because the lab fuses the raw powders in graphite crucibles, all the Fe is converted to ferrous iron prior to analysis, and Fe is reported as FeO*. For plotting purposes, FeO* was recast as FeO = FeO* × 0.85 and Fe_2O_3 = (FeO* - FeO) × 1.1113 where necessary (Ragland, 1989). Two thin sections, one each from sample RRM-14-01 and RRM-14-21, were selected for microprobe analysis using the Cameca SX-100 electron microprobe at the New Mexico Bureau of Geology and Mineral Resources. These samples were collected at the distal ends of the dike to investigate whether there were demonstrable differences in mineral chemistry along the dike.

Modeling Methods

The melting of a presumed spinel lherzolite source was modeled using the equations of Shaw (2006). Distribution coefficients are from McKenzie and O'Nions (1991). Spinel lherzolite rare earth element (REE) values are from McDonough (1990). Chondrite normalization values are from Sun and McDonough (1989). Kilbourne Hole mineralogy (55% olivine, 17% clinopyroxene, 25% orthopyroxene, and 3% spinel) is from Perkins and Anthony (2011).

Results

Petrography and Mineralogy

Railroad Mountain dike samples are uniformly fine-grained and unaltered except for minor local effects, discussed below. Three fundamental textural variations (Types I, II, and III) were observed in thin sections and are shown in Figure 9. Modal analysis by point counting 750 points per slide was consistent among the Type I and II textures, yielding approximately 60% plagioclase, 20% augite, 10% olivine, and 10% opaques (magnetite and ilmenite). Accessory apatite makes up a relatively small volume of the rocks.

Type I: Fine-grained diabasic/trachytic texture dominated by lath-shaped, subhedral plagioclase and scattered larger anhedral plagioclase grains. The rocks are holocrystalline intergranular with anhedral interstitial augite and numerous smaller scattered grains of anhedral olivine and subhedral magnetite. Samples display a moderate to strong flow foliation and are representative of the majority of samples studied in thin section.

Type II: Diabasic texture is somewhat coarser-grained than Type I texture. These samples are dominated by larger, zoned anhedral plagioclase accompanied by a subequal proportion of lath-shaped plagioclase with local parallel alignment. The rocks are holocrystalline intergranular with

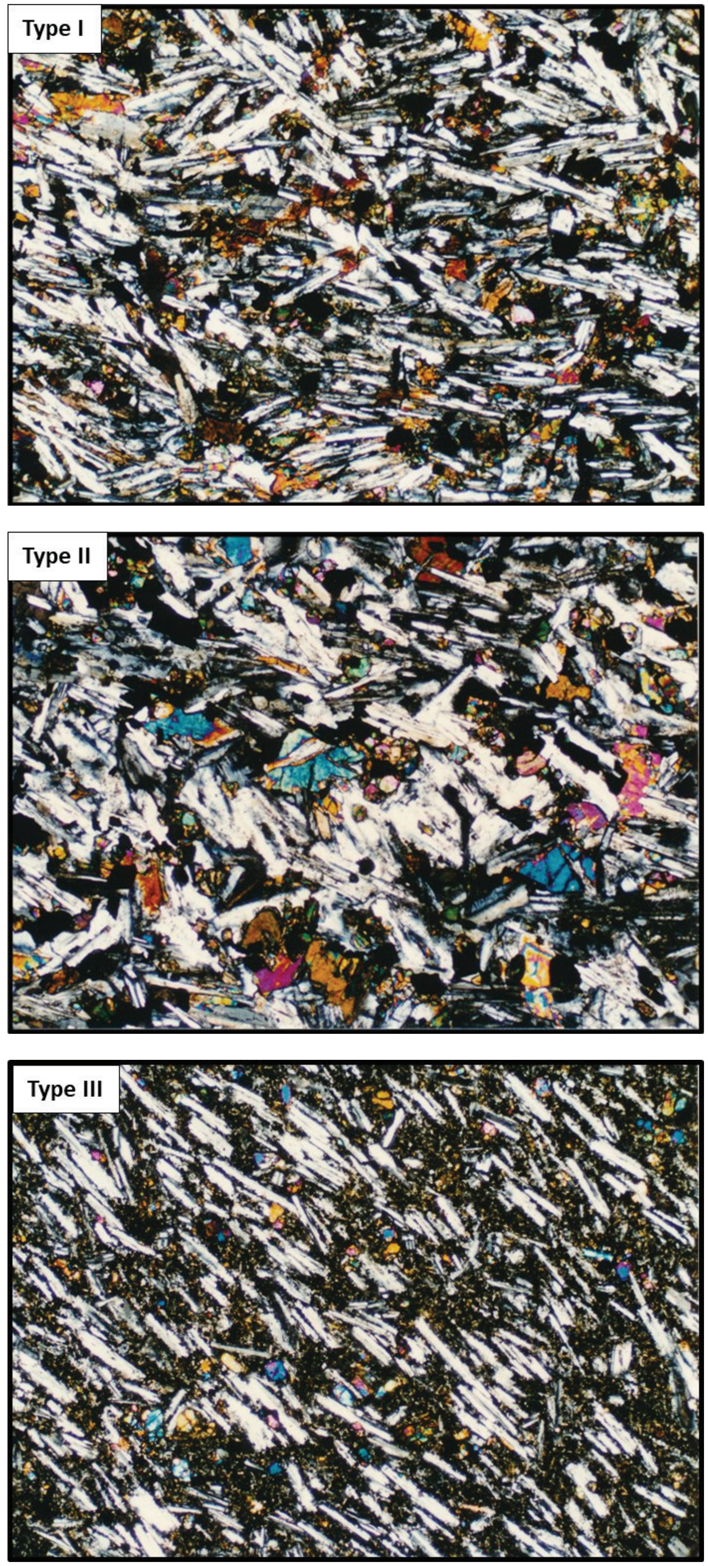

Figure 9. Thin-section photomicrographs taken in cross-polarized light showing the three fundamental textures of the Railroad Mountain dike rocks (field of view is 3.5 mm). **Top:** Type I texture shows lath-shaped plagioclase with scattered grains of olivine, clinopyroxene, and opaques. The parallel orientation of the plagioclase laths is moderately well developed in the center of the photomicrograph. **Middle:** Type II texture is coarser-grained, reflecting slower cooling. Alignment of lath-shaped plagioclase is less well developed than in Type I. **Bottom:** Type III texture occurs closer to the outer margin of the dike and is dominated by appreciably finer-grained plagioclase, mafics, and opaques. The parallel orientation of the plagioclase laths (trachytic texture) is well developed.

[1] Tables are available for download at https://geoinfo.nmt.edu/repository/index.cfml?rid=20250001

anhedral interstitial augite and numerous scattered grains of anhedral olivine and subhedral magnetite. Clinopyroxene and olivine are somewhat coarser-grained. These rocks are from the central portion of the dike and reflect slower cooling compared to the Type I texture.

Type III: A finer-grained variant of the Type I texture forms the margins of the dike. These samples are dominated by very fine-grained, lath-shaped, subhedral plagioclase microlites and a matrix consisting primarily of very fine-grained anhedral grains of augite, olivine, and abundant magnetite. A few random larger grains are present. The rocks are holocrystalline with isolated zones of fine-grained alteration and reflect more rapid cooling.

Plagioclase is generally unaltered except for minor argillic alteration. The subhedral lath-shaped grains are not zoned, but some larger anhedral grains display zoning. Random larger grains are poikilitic, enclosing mostly olivine. The maximum albite twin extinction angle of 30° corresponds to approximately An_{50}. In samples with larger anhedral grains, these grains appear to have crystallized before the lath-shaped grains. Augite is generally anhedral with a small number of subhedral grains. Grains are moderately pleochroic with interference colors indicative of titanaugite. The 2V angle is about 60°, indicating a high-Ca clinopyroxene. Simple twins are common. Rare grains are subophitic. Olivine grains are typically anhedral and finer-grained than augite. Though generally unaltered, a small proportion of grains are altered to green iddingsite. Subhedral magnetite and ilmenite are relatively abundant (about 10%). Some grains display minor local hematitic alteration. Apatite is scattered throughout primarily as blocky and acicular grains.

Microprobe Analyses

Nine olivine and 10 pyroxene grains were analyzed across two thin sections by microprobe, and the compositions were calculated using Gabbrosoft's OLICALC and PYXCALC spreadsheets (http://www.gabbrosoft.org). The analytical results are listed in Table 1 and illustrated in Figure 10. The average olivine composition is $Fo_{49.0}Fa_{49.8}Tp_{1.2}$ and yielded an average liquid composition of XFeO(l)/XMgO(l) = 3.39. The average clinopyroxene composition is $Wo_{43.1}En_{38.4}Fs_{16.7}Ac_{1.7}$.

Eight magnetite and nine ilmenite grains were also analyzed (Table 1). Magnetite-ilmenite geothermometer temperatures and oxygen fugacity were calculated using the ILMAT geothermobarometry spreadsheet of Lepage (2003). The data yielded an average temperature of 1209°C and $\text{Log}_{10} fO_2$ = -7.31, which plots just above the NNO buffer (Fig. 11).

Whole-Rock Geochemistry

Major element oxide concentrations are remarkably consistent across textural variations, with differences between minimum and maximum concentrations less than 1 wt% for all oxides. This excludes three altered samples collected adjacent to contacts (discussed below). There are no vertical or horizontal trends in the composition of these rocks. The SiO_2 concentration ranges from 47.19 to 47.86 wt%, with a mean of 47.51 wt%. Concentrations of FeO* (12.18–12.75 wt%) and MgO (4.81–5.22 wt%) vary by only 0.57 and 0.41 wt%, respectively. The alkalis Na_2O (3.87–4.13 wt%) and K_2O (1.48–1.71 wt%) show even less variation. Variation in MnO (0.01 wt%) and P_2O_5 (0.1 wt%) is negligible.

Samples RRM-7, 8, and 23 are altered and have lower unnormalized totals ranging from 92.30 to 95.58 wt% (Table 2). These samples were not used in plotting. For the remaining samples, LOI (loss on ignition) values averaged 0.56 wt%. Compared to the mean values of the other 37 samples, RRM-7 and 8 are noticeably lower in SiO_2, MnO, CaO, and K_2O. These two samples, collected adjacent to the contact in one of the quarries, are highly oxidized and hematitic, with very few unaltered mafic grains remaining (sample RRM-8 is on the right in Fig. 6). Sample RRM-23 (left, Fig. 6) is noticeably higher in SiO_2, Na_2O, and K_2O and noticeably lower in TiO_2, FeO*, and P_2O_5. Both samples are “spotted” with small vugs filled with clay and calcite.

Ten samples were collected along the walls of a quarry at the western end of the sample area (Fig. 8 and Table 2). The quarry is about 20 m deep and 30 m wide. Although there were slight chemical differences in the samples from the two sides of the quarry, the variation was within analytical error.

The Railroad Mountain rocks plot in a tight cluster in the trachybasalt field (Fig. 12) in the total alkali-silica diagram of Le Maitre et al. (2002) after Le Bas et al. (1986). They are nepheline normative and belong to the sodic alkali olivine basalt series (Fig. 13) of Irvine and Baragar (1971). The rocks have been previously described as olivine gabbro (Semmes, 1920), medium-grained olivine gabbro (Kelley, 1971), and a fine-grained, equigranular olivine syenogabbro (Allen and Foord, 1991). Based on petrographic characteristics and modal mineralogy, the rocks are olivine diabase. Geochemically, they are sodic alkali trachybasalts.

Mg#s ($100 \times Mg^{2+}/(Mg^{2+} + Fe^{2+})$), a proxy for fractionation (Rollinson and Pease, 2021), range from 40.93 to 43.30, with a mean of 41.84, and are plotted against major element oxides and selected trace elements in Figures 14A and 14B, respectively. The trend of Mg# versus SiO_2 is essentially flat and not unexpected for these rocks. The concentrations of TiO_2, FeO*, CaO, and Sc increase with decreasing Mg#, suggesting clinopyroxene fractionation. The decrease in Cr and Ni with decreasing Mg# likely reflects changes in olivine composition during differentiation. The low Mg#s and very low Cr concentrations (average = 13.07 ppm) suggest significant differentiation prior to intrusion. This process is also indicated by the increase in Sr and decrease in Sc (Fig. 14B). Differentiation was dominated by clinopyroxene removal with minimal plagioclase and olivine fractionation.

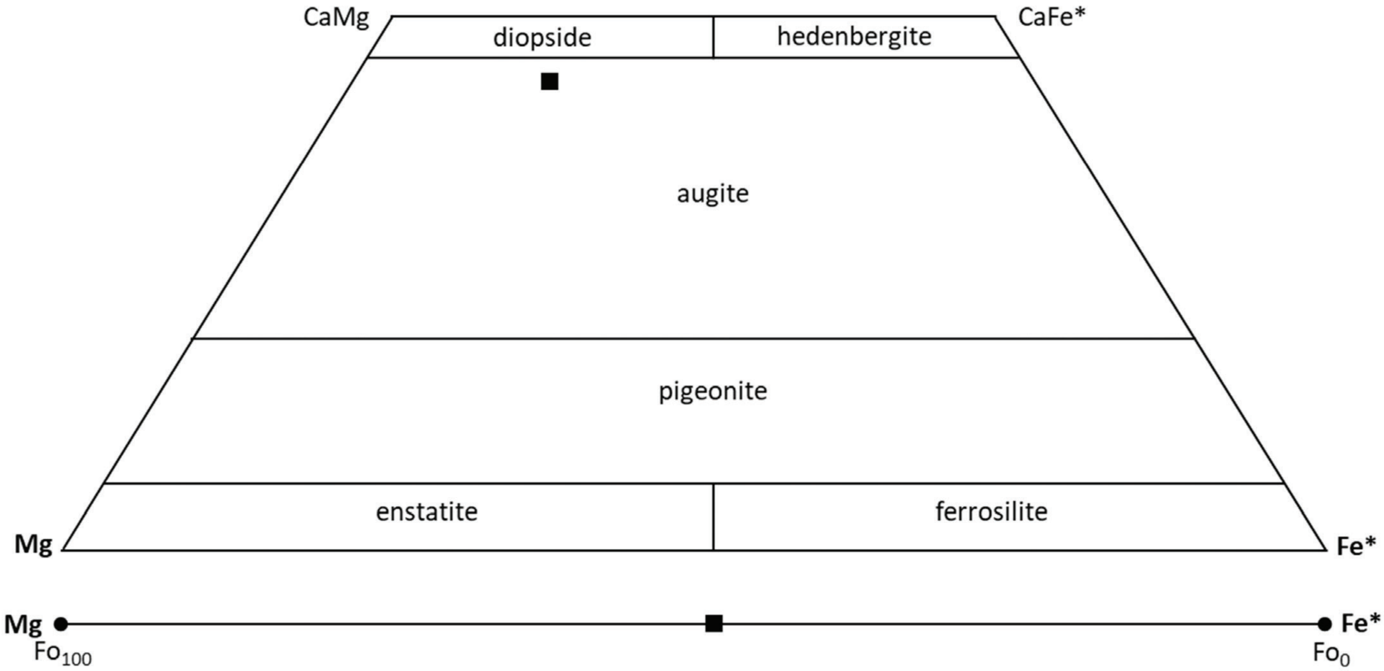

Figure 10. The pyroxene quadrilateral diagram shows the average clinopyroxene composition (upper square) corresponding to $Wo_{43.1}En_{38.4}Fs_{16.7}Ac_{1.7}$. The linear composition bar below shows the average olivine composition (lower square) of $Fo_{49.0}Fa_{49.8}Tp_{1.2}$. Compositions were recalculated from electron microprobe analyses.

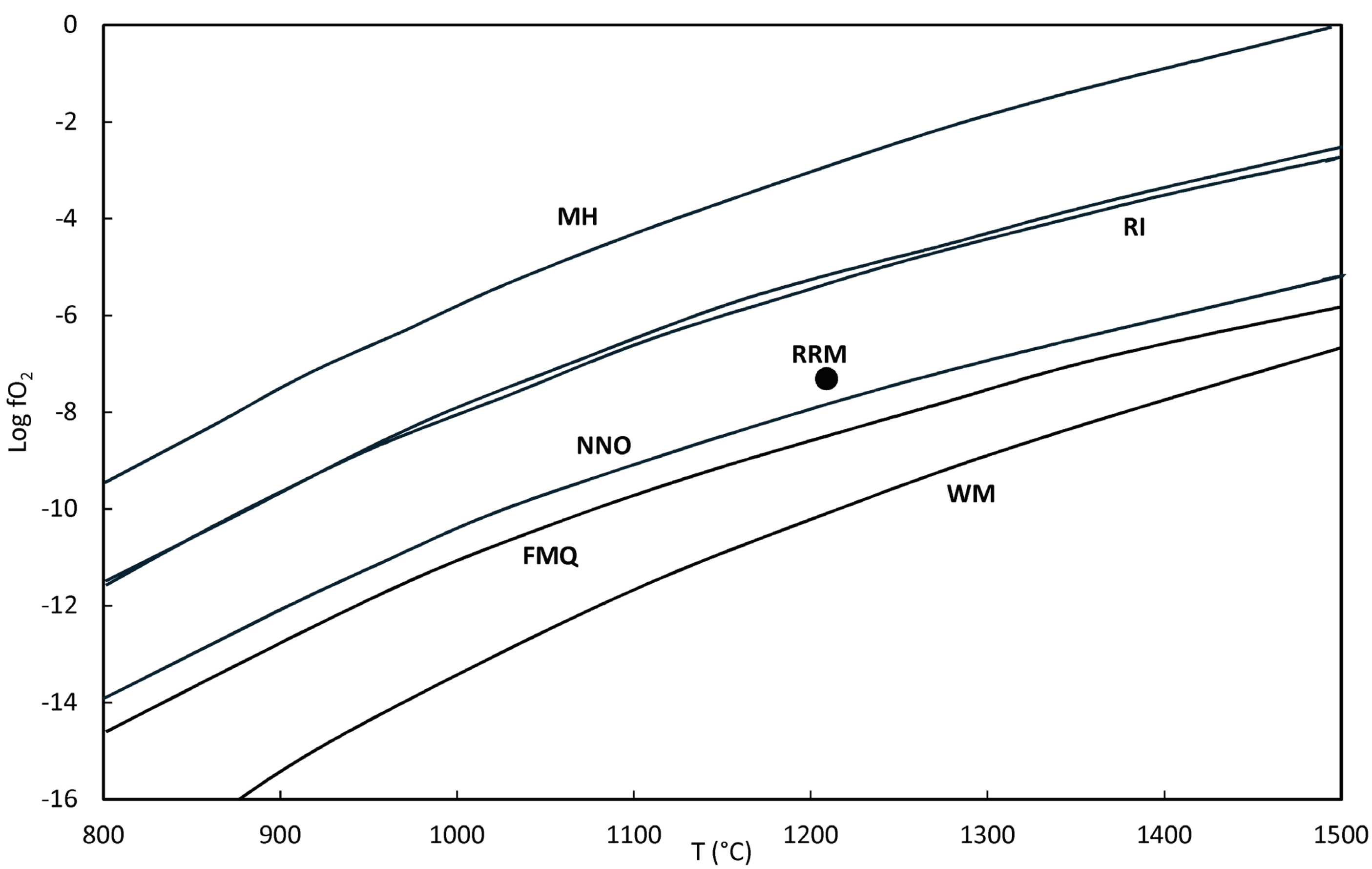

Figure 11. Oxygen fugacity and Fe-Ti oxide equilibrium temperatures were calculated using the ILMAT geothermobarometry spreadsheet of Lepage (2003). Railroad Mountain (RRM) plots on the right (circle), just above the nickel-nickel oxide (NNO) buffer curve. The other buffer curves are magnetite-hematite (MH), rutile-ilmenite (RI), fayalite-magnetite-quartz (FMQ), and wüstite-magnetite (WM).

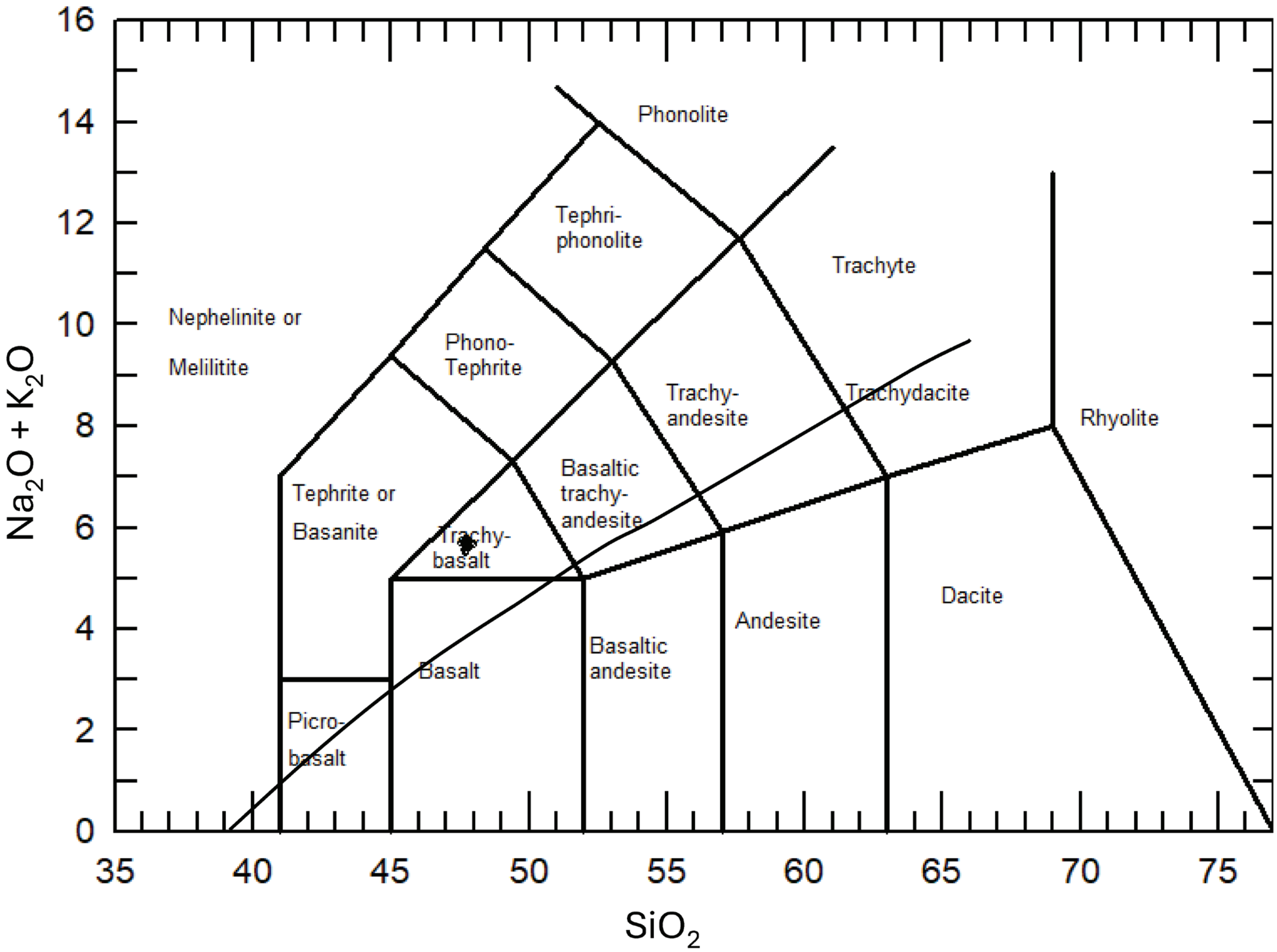

Figure 12. Total alkali-silica diagram of Le Maitre et al. (2002) after Le Bas et al. (1986). Note the lack of variation in silica and alkalis for Railroad Mountain (tight cluster of crosses). The alkalic-subalkalic boundary is from Irvine and Baragar (1971).

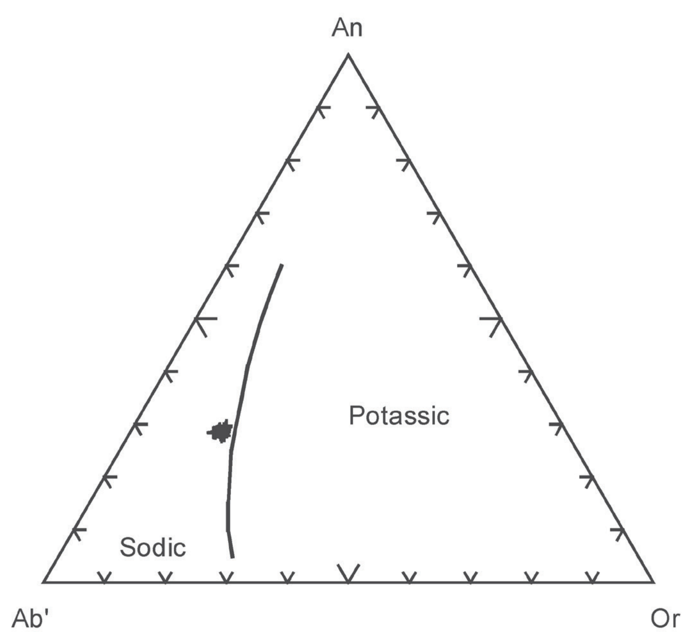

Figure 13. The Railroad Mountain rocks plot in the sodic series field of the Ab'-An-Or ternary diagram of Irvine and Baragar (1971).

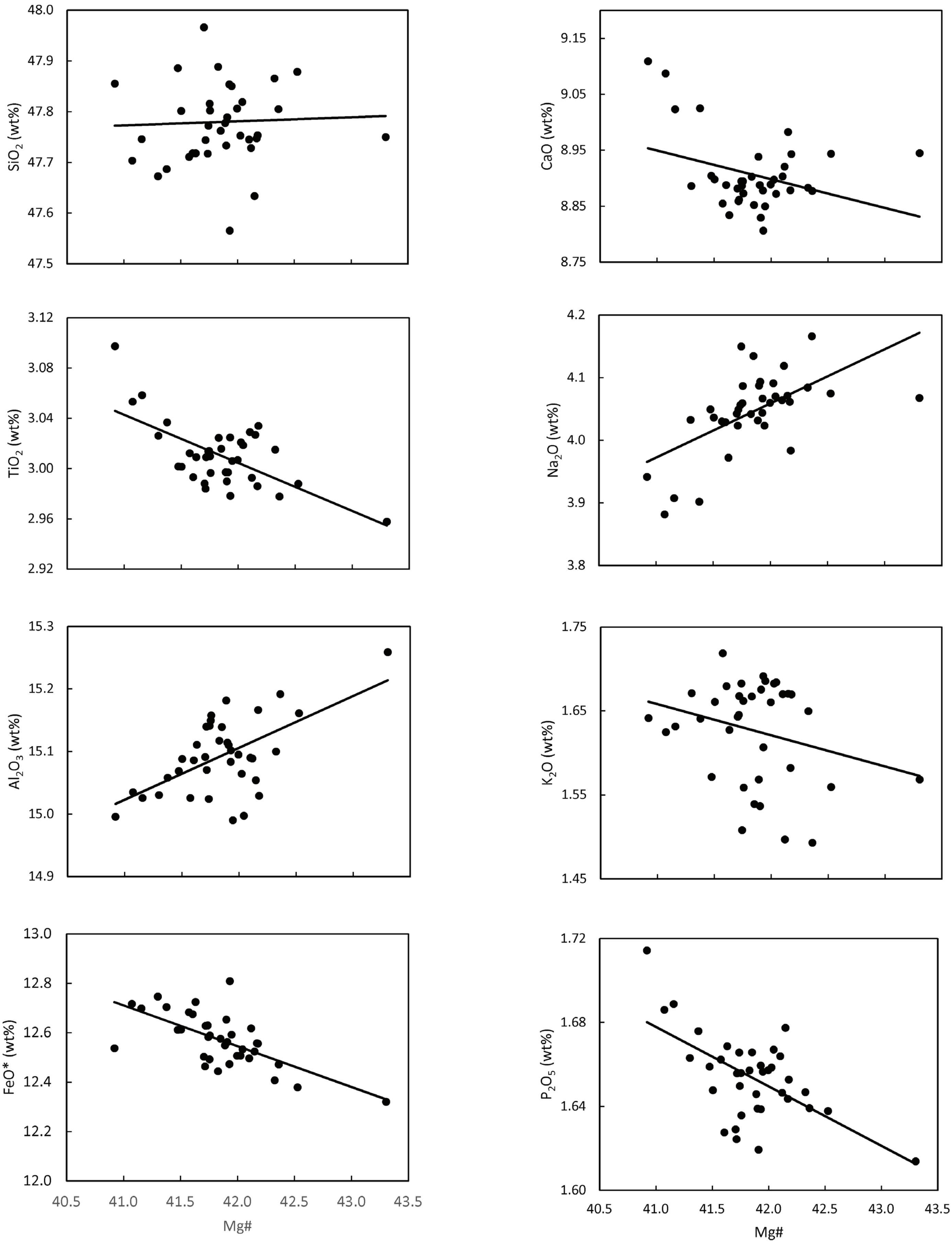

Figure 14A. Mg# ($100 \times Mg^{2+}/(Mg^{2+} + Fe^{2+})$) plotted against selected major oxides.

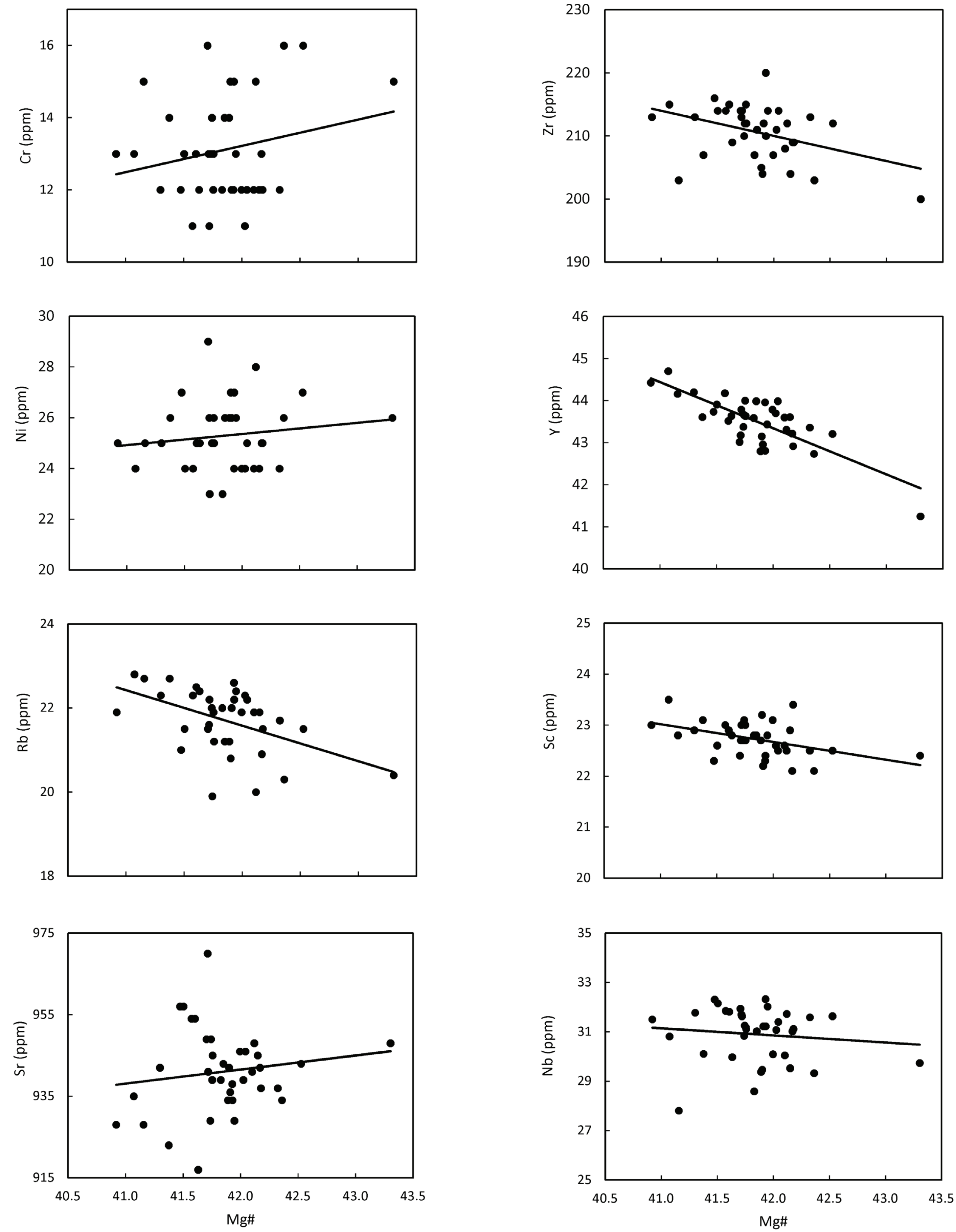

Figure 14B. Mg# (100 × Mg^{2+}/(Mg^{2+} + Fe^{2+})) plotted against selected trace elements.

Trace element concentrations are also remarkably consistent, averaging about ± 3 ppm, with only Ba, Sr, and Zr showing significant variation. The REEs were normalized using the chondrite values of Sun and McDonough (1989) and are plotted in Figure 15. There is virtually no variation in the values, and all samples plot in a tight cluster. The light REEs (LREE) are moderately enriched (La/Yb_N = 12.72–13.26), with minimal heavy REE (HREE) enrichment (Tb/Yb_N = 2.37–2.48) and negligible Eu anomalies (Eu/Eu* = 0.94–0.98). The elevated LREE concentrations and the minor HREE fractionation suggest an asthenospheric mantle source that experienced a metasomatic event prior to eruption (Mysen and Holloway, 1977; Allen and Ford, 1991). Garnet is always richer in HREEs relative to LREEs because of larger distribution coefficients for the HREEs in garnet, which leads to extreme fractionation (Rollinson and Pease, 2021). Previous workers, including Faris (1980) and Baldridge (1979), have proposed that spinel lherzolites are the likely source material for alkaline basalts in the Rio Grande rift. Furthermore, Perkins and Anthony (2011) modeled pressure estimates for Kilbourne Hole spinel lherzolites, which placed the estimates in the spinel stability field at depths of 30–45 km. This is above the 60-km-deep spinel-garnet transition in the mantle.

Apatite appears to have been important in controlling REE concentrations. Figure 16 shows P_2O_5 concentration increasing with increasing Nd concentration. Except for Ce, Gd, Tm, and Lu, all of the other REEs show identical trends. Apatite and other REE-rich accessory minerals are common in metasomatized mantle xenoliths, and their alkalic host rocks control their REE patterns (Allen and Foord, 1991). Allen and Foord (1991) report that other rocks of the Lincoln County porphyry belt are enriched in LREEs. The epsilon Nd values are near "bulk earth," indicating that enrichment and metasomatism occurred just prior to magma generation since, over time, high Nd/Sm ratios would yield lower epsilon Nd values (Allen and Foord, 1991). Evidence that metasomatism (elevated concentrations of fluid-mobile elements and LREE enrichment) occurs in the mantle just prior to magma generation has been documented in other alkaline provinces (Menzies and Murthy, 1980; Futa and Armbrustmacher, 1987; Roden, 1987).

The spider diagram (Fig. 17) was generated using the primitive mantle values of McDonough and Sun (1995). The large ion lithophile elements (LILEs) are enriched 26 to 160 times primitive mantle values, and the high field strength elements (HFSEs) are enriched 14 to 98 times primitive mantle values. The overall pattern does show that the LILEs Rb, K, Sr, and Eu and the HFSEs Nb, Ta, Zr, Hf, and Ti are depleted relative to other values. Barium is enriched by an average of 160 times primitive mantle values, which may be the result of mantle metasomatism (Allen and Foord, 1991; Humphreys et al., 2003). The only element to exhibit any variation in the spider diagram is Cs. The reason for this variation is unclear, but it may be related to metasomatism as a result of fluxing of the overlying mantle caused by the devolatilization of minerals in the subducted Farallon plate (Allen and Foord, 1991; Humphreys et al., 2003). Li et al. (2019) showed that Cs can be adsorbed on the surface of 2:1 clays, such as illite and smectite, which may have been added to the lithosphere during the dehydration of the Farallon slab. The moderate incompatible element enrichment may indicate the lack of previous melt extraction in the source rocks. The negative Pb anomaly and the lack of enrichment of Nb and Ta suggest limited crustal contamination. Plots of Nb-Ta, Nb-Hf, Nb-Zr, and Zr-Hf (Fig. 18) show strong interelement correlation, which may be controlled by ilmenite crystallization.

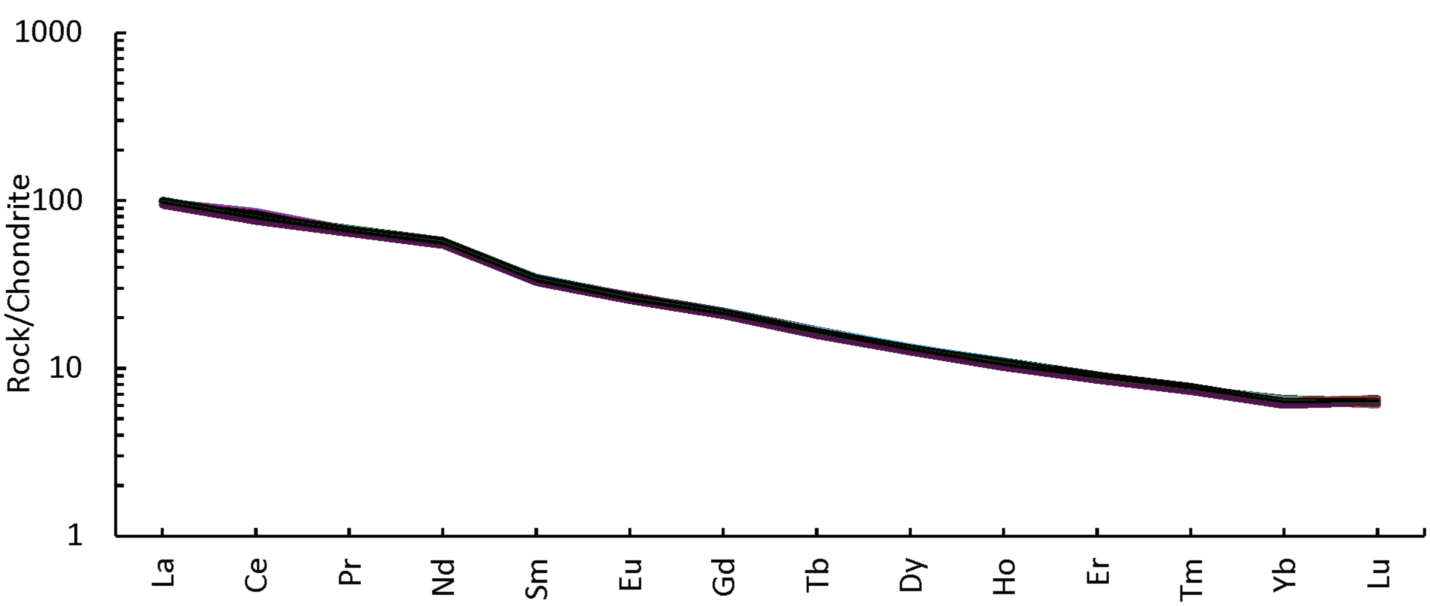

Figure 15. Chondrite-normalized REE plot. Normalization values are from Sun and McDonough (1989). Note the lack of variation between samples.

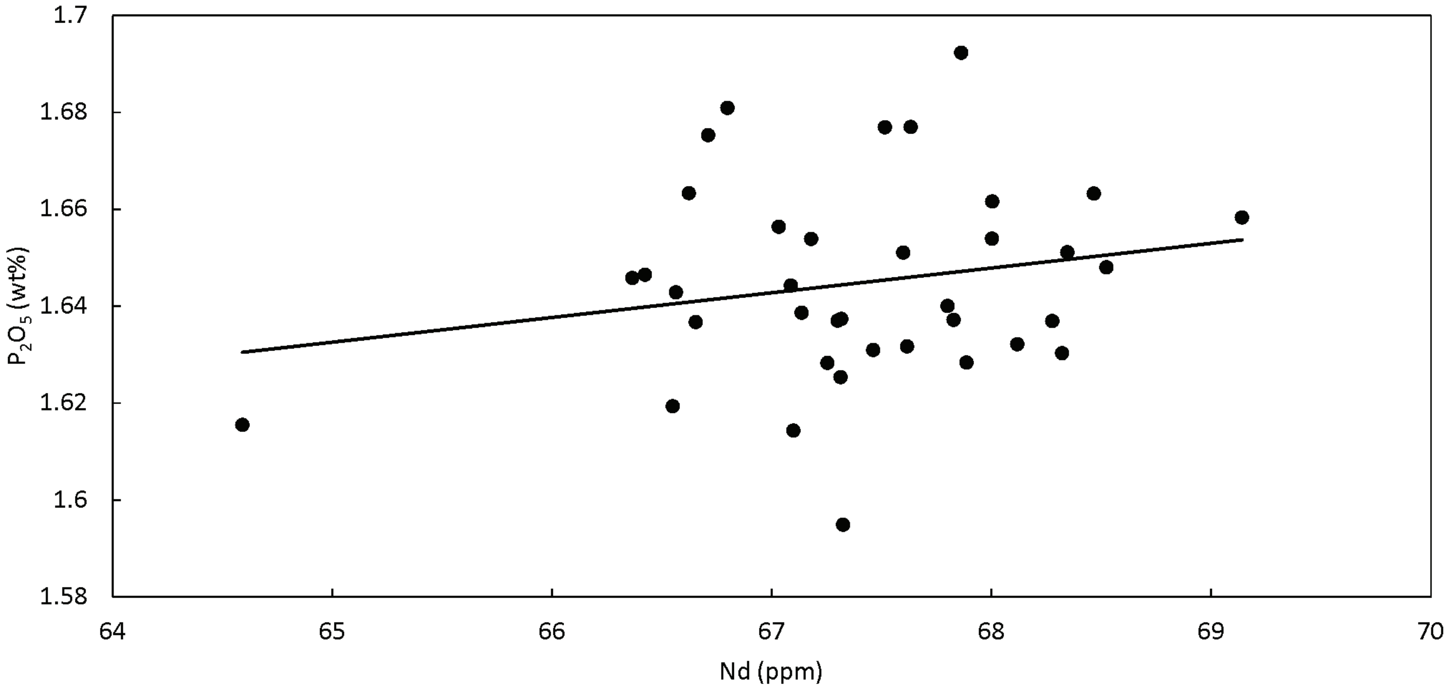

Figure 16. Plot of P_2O_5 versus Nd indicates that apatite probably played a strong role in controlling REE concentrations. All the REEs show the same relationship of increasing concentration with increasing P_2O_5 concentration.

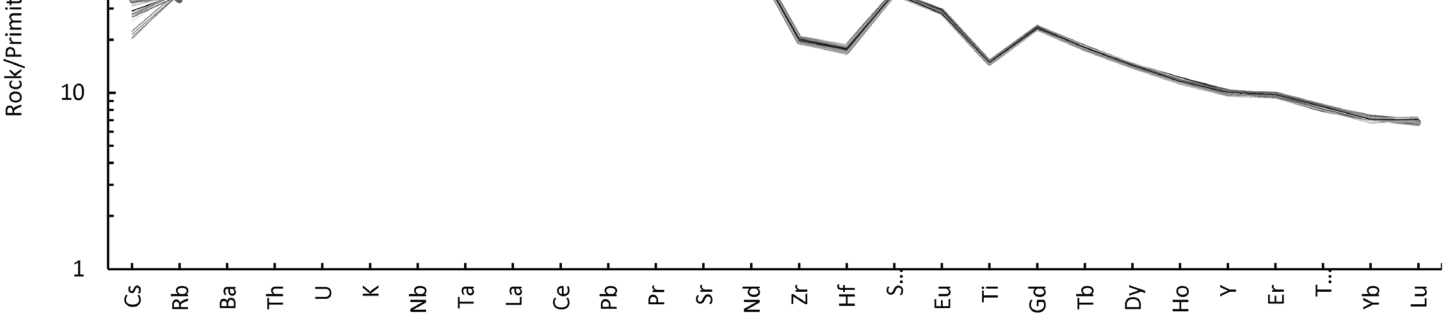

Figure 17. Primitive mantle-normalized spider plot. Normalization values are from McDonough and Sun (1995). Cesium is the only element to exhibit any significant variation, which may be due to metasomatism of the mantle caused by the devolatilization of minerals in the subducted Farallon plate (Allen and Foord, 1991; Humphreys et al., 2003; Li et al., 2019).

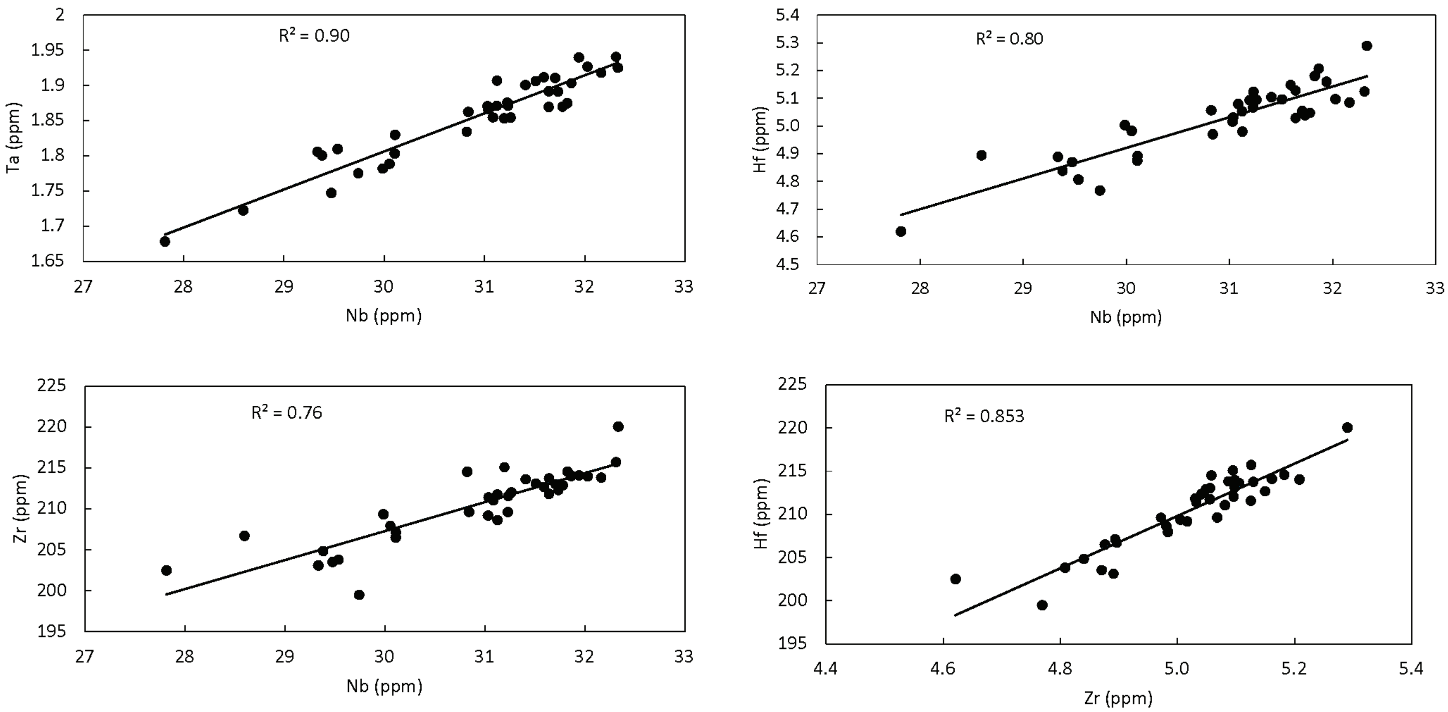

Figure 18. Plots of high field strength elements Nb-Ta, Nb-Hf, Nb-Zr, and Zr-Hf show a strong correlation, possibly controlled by ilmenite during crystallization.

Petrogenesis

Allen and Foord (1991) reported an initial $^{87/86}Sr$ ratio of 0.70411 and an εNd value of +0.5 for Railroad Mountain, which plots close to the lower limit of the mantle array at less radiogenic values than bulk earth (Fig. 19). The Sr and Nd isotope ratios are consistent with a primitive mantle melt. However, the LREE values indicate modification (enrichment) of the mantle. Most workers agree that isotopic evidence indicates that sodic alkali basalts require parental magmas dominated by components from the sublithospheric mantle. The uncertainty is whether these magmas are derived directly from sublithospheric mantle melting or from the melting of mantle that had been metasomatized by "incompatible element enriched fluids/melts derived from small degrees of melting of upwelling asthenosphere" (Farmer, 2014).

The lack of HREE fractionation displayed on the chondrite-normalized REE plot (Fig. 15) is inconsistent with a garnet-bearing source. The likely source was spinel-bearing at a depth of less than 80 km (Wyllie, 1981; Ellam, 1992; Takahashi et al., 1993; Hirschmann and Stolper, 1996). Baldridge (1979) reported that alkali olivine basalts of the central Rio Grande rift could be derived from 10% partial melting of spinel pyrolite at 50–70 km depth. Spinel lherzolite mantle xenoliths occur in the Rio Grande rift at Kilbourne Hole, New Mexico, located in the Potrillo volcanic field, approximately 340 km southwest of Railroad Mountain. Satsukawa et al. (2011), using phase relations and the temperature of equilibration, concluded that the xenoliths at Kilbourne Hole were derived from depths of 35–60 km.

The melting of a presumed spinel lherzolite source was modeled using the equations of Shaw (2006). Distribution coefficients are from McKenzie and O'Nions (1991, table 3). Spinel lherzolite REE values are from McDonough (1990, table 1). Chondrite normalization values are from Sun and McDonough (1989). Kilbourne Hole mineralogy (55% olivine, 17% clinopyroxene, 25% orthopyroxene, and 3% spinel) is from Perkins and Anthony (2011, table 3). The results of nonmodal equilibrium and nonmodal fractional batch melting models are similar and are shown in Figure 20. The uniform chemistry of the Railroad Mountain rocks suggests that nonmodal equilibrium batch melting may have been more likely than nonmodal fractional batch melting (Shaw, 2006). The results indicate a small degree (around 5%) of partial melting of a spinel lherzolite parent, which is consistent with what other workers have reported (Farmer, 2014). The models are consistent with the results obtained with IgPet 2017 software using the equations of Albarède (1995).
The much younger (about 5 ka) Carrizozo basalt field lies at the western end of the Lincoln County porphyry belt (Fig. 1). Faris (1980) reported that the Carrizozo basalts formed by 4–6% partial melting of a spinel-peridotite parent, which is consistent with the results obtained in this study.

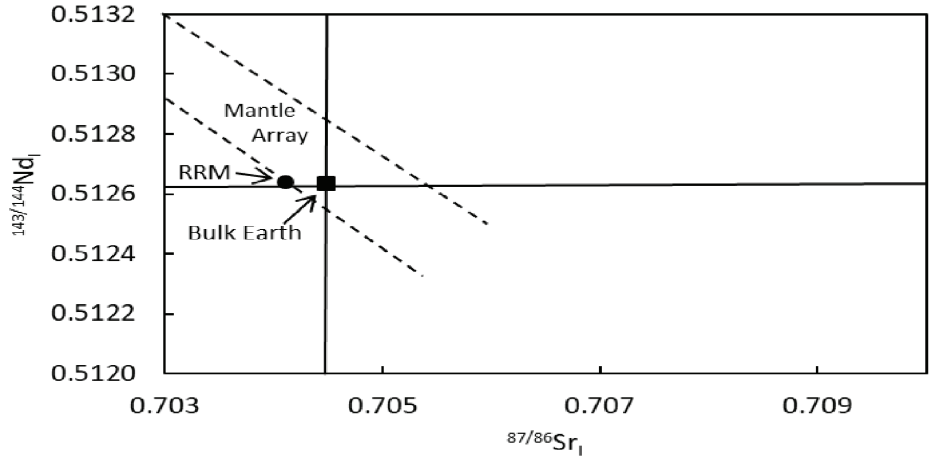

Figure 19. Initial $^{87/86}Sr$ and $^{143/144}Nd$ isotope ratios (circle) for Railroad Mountain (from Allen and Foord, 1991). Railroad Mountain plots on the lower boundary of the mantle array at less radiogenic initial $^{87/86}Sr$ values, close to bulk earth ratios (square).

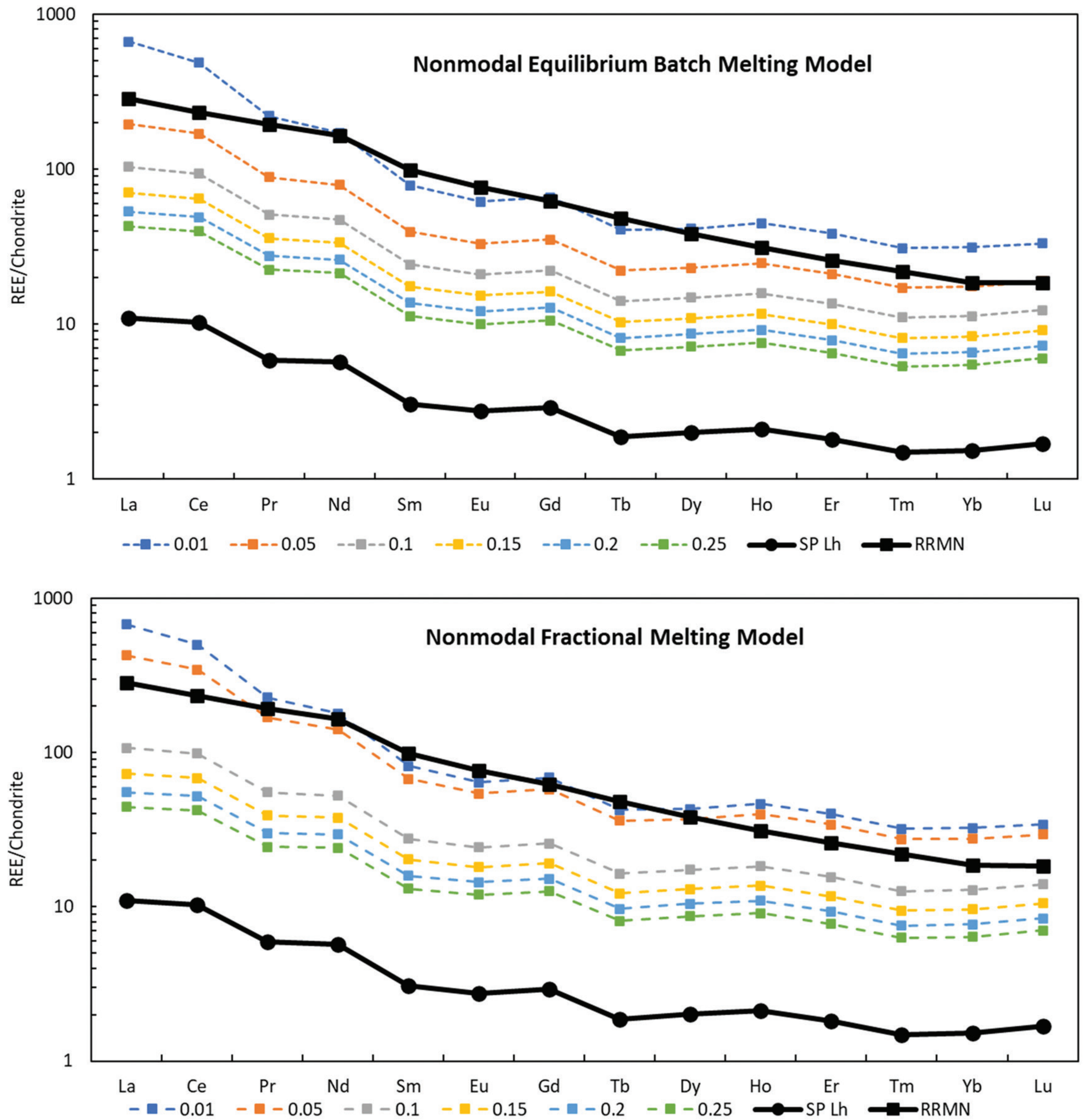

Figure 20. Nonmodal equilibrium (top) and nonmodal fractional (bottom) melting models for Railroad Mountain indicate approximately 5% melting of a spinel lherzolite source using the equations of Shaw (2006). Spinel lherzolite REE values are from McDonough (1990, table 1). Chondrite normalization values are from Sun and McDonough (1989). Kilbourne Hole spinel lherzolite mineralogy (55% olivine, 17% clinopyroxene, 25% orthopyroxene, and 3% spinel) is from Perkins and Anthony (2011, table 3).

Tectonics

All of the Railroad Mountain samples plot in the within-plate field on the Zr–Zr/Y tectonic discrimination diagram (Fig. 21) of Pearce and Norry (1979). The Railroad Mountain dike was intruded at the edge of the stable North American craton following the foundering and tearing of the Farallon slab (Fig. 22). During the Cretaceous, the steep dip of the Farallon plate was responsible for producing a wide magmatic arc along the west coast of North America (Dickinson, 2009). The Farallon slab was in contact with the lithosphere beneath North America, and dewatering of the slab and sediments (Hole et al., 1984; Othman et al., 1989) hydrated the base of the lithosphere (Humphreys et al., 2003; Ricketts et al., 2016). These fluids infiltrated and metasomatized the overlying mantle wedge (Fitton et al., 1991). The elevated concentrations of fluid-mobile elements, such as Cs, Ba, Th, and Pb (Fig. 17), are likely the result of metasomatism during slab dewatering (Chang et al., 2009)

Previous workers (Coney and Reynolds, 1977; Humphreys, 1995, 2009; Dickinson, 2009) have suggested that the Farallon flat slab was in place until at least 45 Ma. This was followed at about 40 Ma by slab rollback, delamination from the North American lithosphere, and subsequent foundering of the slab, which exposed the metasomatized North American lithosphere to the underlying hot asthenosphere (Humphreys et al., 2003; Ricketts et al., 2016). In the region east of the Rio Grande rift, volcanic activity in the Sierra Blanca volcanic field at the eastern end of the Lincoln County porphyry belt was underway by about 37 Ma (Constantopoulos, 2007). Tearing of the slab beneath central New Mexico between 25 and 30 Ma, as suggested by Ricketts et al. (2016, p. 418), may have linked previously foundered portions with final slab detachment, intensifying asthenospheric upwelling (Fig. 22). The timing would correspond to the age of Railroad Mountain (27.66 ± 0.03 Ma) and the start of Rio Grande rifting.

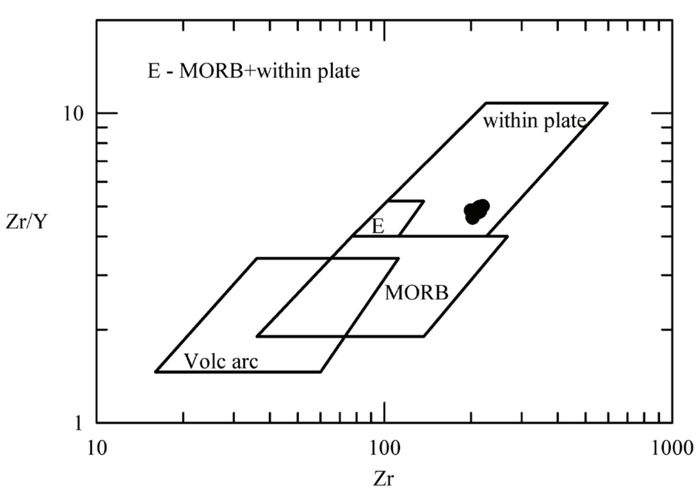

Figure 21. Zr versus Zr/Y tectonic discrimination diagram of Pearce and Norry (1979). The samples plot as a tight cluster in the within-plate field.

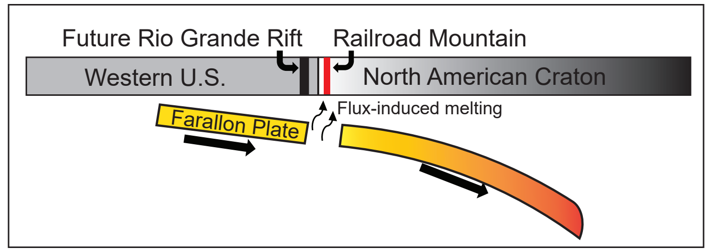

Figure 22. Simplified tectonic model at the time of intrusion of the Railroad Mountain dike at 27.66 Ma, which was intruded at the edge of the stable North American craton. By this time, the Farallon plate had detached from the lithosphere, and the portion beneath central New Mexico had torn, enabling asthenospheric upwelling and the generation of magmatic activity in the Lincoln County porphyry belt. Rio Grande rifting began shortly thereafter at about 25 Ma (Ricketts et al., 2016).

Conclusions

This work presents new mineralogical, geochemical, geochronological, and petrogenetic information on the Railroad Mountain dike, adding to our understanding of the region adjacent to the Rio Grande rift. The rocks are uniformly fine-grained, are diabasic to diabasic/trachytic, and average 60% plagioclase (approximately An_{50}), 20% Ti-rich augite, 10% olivine (approximately Fo_{49}), 10% opaques (magnetite and ilmenite), and accessory apatite. Magnetite-ilmenite geothermometer temperatures and oxygen fugacity data yielded an average temperature of 1209°C and $Log_{10} fO_2$ of -7.31. Petrographically, the rocks are an olivine diabase. Two new groundmass $^{40}Ar/^{39}Ar$ age determinations averaged 27.66 ± 0.03 Ma.

Major element oxide concentrations are remarkably consistent, with minimal variation. Mg#s range from 40.93 to 43.30, with a mean of 41.84. The rocks plot in the trachybasalt field on the total alkali-silica plot. They are nepheline normative and belong to the sodic alkali olivine basalt series. Geochemically, they are sodic alkali trachybasalts. The concentrations of TiO_2, FeO*, CaO, and Sc increase with decreasing Mg#, suggesting clinopyroxene fractionation. The decrease in Cr and Ni with decreasing Mg# likely reflects changes in olivine composition during differentiation. The low Mg#s and very low Cr concentrations suggest differentiation dominated by clinopyroxene removal with minimal plagioclase and olivine fractionation. Trace element concentrations are also remarkably consistent, averaging about ± 3 ppm, with only Ba, Sr, and Zr showing significant variation. There is virtually no variation seen on the chondrite-normalized REE diagram. LREEs are moderately enriched (La/Yb_N = 12.72–13.26), with minimal HREE enrichment (Tb/Yb_N = 2.37–2.48) and negligible Eu anomalies (Eu/Eu* = 0.94–0.98). The lack of HREE fractionation indicates an asthenospheric mantle source with no residual garnet. LILEs are enriched 26 to 160 times primitive mantle values, and the HFSEs are enriched 14 to 98 times primitive mantle values. Barium is enriched by an average of 160 times primitive mantle values, which may be the result of mantle metasomatism. The variation in Cs concentration is possibly from the fluxing of the lithospheric mantle caused by the devolatilization of minerals in the subducted Farallon plate. The negative Pb anomaly and the lack of enrichment of Nb and Ta suggest limited crustal contamination.

The lack of HREE fractionation on the chondrite-normalized REE plot suggests a spinel lherzolite source. Nonmodal equilibrium and nonmodal fractional batch melting models indicate a small degree (~5%) of partial melting of a spinel lherzolite parent. The uniform chemistry of the Railroad Mountain rocks suggests nonmodal equilibrium batch melting. The results are consistent with previous results from the Lincoln County porphyry belt.

The Railroad Mountain dike samples plot in the within-plate field on the Zr–Zr/Y tectonic discrimination diagram. The dike was intruded at the edge of the stable North American craton following the foundering and tearing of the Farallon slab. Dewatering of the slab and sediments hydrated the base of the lithosphere, which metasomatized the overlying mantle wedge. Slab rollback, delamination from the North American lithosphere, and subsequent foundering of the slab at about 40 Ma exposed the metasomatized North American lithosphere to the underlying hot asthenosphere. Tearing of the slab beneath central New Mexico between 25 and 30 Ma may have intensified asthenospheric upwelling, leading to the intrusion of the Railroad Mountain dike as Rio Grande rifting began.

Acknowledgments

A faculty research grant from Eastern New Mexico University funded the whole rock geochemical analyses. Laural Cherednik (Scholl) prepared the first thin sections and did preliminary petrographic descriptions as part of her senior research project. James Hollen assisted in the collection of the first group of samples. Nelia Dunbar (New Mexico Bureau of Geology and Mineral Resources) provided the electron microprobe data. Matt Heizler (New Mexico Bureau of Geology and Mineral Resources) provided the new age dates. Shari Kelley, Richard Chamberlin, and Snir Attia provided helpful comments, which greatly improved the manuscript.

References

Albarède, F., 1995, Introduction to Geochemical Modeling: Cambridge, Cambridge University Press, 543 p. https://doi.org/10.1017/CBO9780511622960

Aldrich, M.J., Jr., Chapin, C.E., and Laughlin, A.W., 1986, Stress history and tectonic development of the Rio Grande Rift, New Mexico: Journal of Geophysical Research, v. 91, no. B6, p. 6199–6211. https://doi.org/10.1029/JB091iB06p06199

Allen, M.S., and Foord, E.E., 1991, Geological, geochemical, and isotopic characteristics of the Lincoln County porphyry belt, New Mexico—Implications for regional tectonics and mineral deposits, *in* Barker, J.M., Kues, B.S., Austin, G.S., and Lucas, S.G., eds., Geology of the Sierra Blanca, Sacramento and Capitan Ranges, New Mexico: New Mexico Geological Society Fall Field Conference Guidebook 42, p. 97–113. https://doi.org/10.56577/FFC-42.97

Allen, M.S., and McLemore, V.T., 1991, The geology and petrogenesis of the Capitan pluton, New Mexico, *in* Barker, J.M., Kues, B.S., Austin, G.S., and Lucas, S.G., eds., Geology of the Sierra Blanca, Sacramento and Capitan Ranges, New Mexico: New Mexico Geological Society Fall Field Conference Guidebook 42, p. 115–127. https://doi.org/10.56577/FFC-42.115

Baldridge, W.S., 1979, Petrology and petrogenesis of Plio-Pleistocene basaltic rocks from the central Rio Grande rift, New Mexico, and their relation to rift structure, *in* Riecker, R.E., ed., Rio Grande rift—Tectonics and magmatism: Washington, D.C., American Geophysical Union, p. 323–354.

Bartsch-Winkler, S., 1992, Geology of east-central New Mexico (with a section on intrusive and extrusive alkaline rocks of the Lincoln County porphyry belt by T.J. Armbrustmacher), *in* Bartsch-Winkler, S., ed., Mineral and energy resources of the BLM Roswell resource area, east-central, New Mexico: U.S. Geological Survey Open-File Report 92-0261, p. 4–42. https://doi.org/10.3133/ofr92261

Carmichael, I.S.E., Turner, F.J., and Verhoogen, J., 1974, Igneous Petrology: New York, McGraw-Hill, 739 p.

Cather, S.M., 1991, Tectonic overview of the Ruidoso region, *in* Barker, J.M., Kues, B.S., Austin, G.S., and Lucas, S.G., eds., Geology of the Sierra Blanca, Sacramento and Capitan Ranges, New Mexico: New Mexico Geological Society Fall Field Conference Guidebook 42, p. 37–39. https://doi.org/10.56577/FFC-42

Chang, J.M., Feeley, T.C., and Deraps, M.R., 2009, Petrogenesis of basaltic volcanic rocks from the Pribilof Islands, Alaska, by melting of metasomatically enriched depleted lithosphere, crystallization differentiation, and magma mixing: Journal of Petrology, v. 50, no. 12, p. 2249–2286. https://doi.org/10.1093/petrology/egp075

Chapin, C.E., Chamberlin, R.M., Osburn, G.R., White, D.W., and Sanford, A.R., 1978, Exploration framework of the Socorro geothermal area, New Mexico, *in* Chapin, C.E., Elston, W.E., and James, H.L., eds., Field guide to selected cauldrons and mining districts of the Datil–Mogollon volcanic field, New Mexico: New Mexico Geological Society Special Publication 7, p. 114–129. https://doi.org/10.56577/SP-7

Coney, P.J., and Reynolds, S.J., 1977, Cordilleran Benioff zones: Nature, v. 270, p. 403–406. https://doi.org/10.1038/270403a0

Constantopoulos, J., 2007, Geochemistry of the Bonito Lake stock, Lincoln County, New Mexico—Petrogenesis and hydrothermal alteration: Rocky Mountain Geology, v. 42, no. 2, p. 137–155. https://doi.org/10.2113/gsrocky.42.2.137

Dickinson, W.R., 2009, Anatomy and global context of the North American Cordillera, *in* Kay, S.M., Ramos, V.A., and Dickinson, W.R., eds., Backbone of the Americas—Shallow subduction, plateau uplift, and ridge and terrane collision: Geological Society of America Memoir 204, p. 1–29. https://doi.org/10.1130/2009.1204(01)

Ellam, R.M., 1992, Lithospheric thickness as a control on basalt geochemistry: Geology, v. 20, no. 2, p. 153–156. https://doi.org/10.1130/0091-7613(1992)020%3C0153:LTAACO%3E2.3.CO;2

Ewing, T.E., 1990, Tectonic map of Texas: Austin, Texas Bureau of Economic Geology, scale 1:750,000, 4 sheets.

Faris, K.B., 1980, A geochemical model for the magmatic history of the Carrizozo basalt field, south-central New Mexico [MS thesis]: Socorro, New Mexico Institute of Mining and Technology, 168 p.

Farmer, G.L., 2014, Continental basaltic rocks, *in* Holland, H.D., and Turekian, K.K., eds., Treatise on Geochemistry (second edition), p. 75–110. https://doi.org/10.1016/B0-08-043751-6/03019-X

Fisher, C.A., 1906, Preliminary report on the geology and underground waters of the Roswell artesian area, New Mexico: U.S. Geological Survey Water Supply Paper 158, 29 p. https://doi.org/10.3133/wsp158

Fitton, J.G., James, D., and Leeman, W.P., 1991, Basic magmatism associated with Late Cenozoic extension in the western United States—Compositional variation in space and time: Journal of Geophysical Research, v. 96, no. B8, p. 13693–13711. https://doi.org/10.1029/91JB00372

Futa, K., and Armbrustmacher, T.J., 1987, Combined Rb/Sr and Sm/Nd systems study on three alkaline intrusive complexes in northwestern Montana, *in* Morris, E.M., and Pasteris, J.D., eds., Mantle metasomatism and alkaline magmatism: Geological Society of America Special Paper 215, 376 p. https://doi.org/10.1130/SPE215

Goff, F., Roback, R.C., McIntosh, W., Goff, C.J., and Kluk, E.C., 2014, Geochemistry and geochronology of intrusive and volcanic rocks of the Three Rivers stock, Sierra Blanca, New Mexico, *in* Rawling, G., McLemore, V.T., Timmons, S., and Dunbar, N., eds., Geology of the Sacramento Mountains Region: New Mexico Geological Society Fall Field Conference Guidebook 65, p. 183–196. https://doi.org/10.56577/FFC-65.183

Hirschmann, M.M., and Stolper, E.M., 1996, A possible role for garnet pyroxene in the origin of the “garnet signature” in MORB: Contributions to Mineralogy and Petrology, v. 124, p. 185–208. https://doi.org/10.1007/s004100050184

Hole, M.J., Saunders, A.D., Marriner, G.F., and Tamey, J., 1984, Subduction of pelagic sediments—Implications for the origin of Ce-anomalous basalts from the Mariana Islands: Journal of the Geological Society of London, v. 141, no. 3, p. 453–412. https://doi.org/10.1144/gsjgs.141.3.0453

Humphreys, E., 1995, Post-Laramide removal of the Farallon slab, western United States: Geology, v. 23, no. 11, p. 987–990. https://doi.org/10.1130/0091-7613(1995)023%3C0987:PLROTF%3E2.3.CO;2

Humphreys, E., 2009, Relation of flat slab subduction to magmatism and deformation in the western United States, *in* Kay, S.M., Ramos, V.A., and Dickinson, W.R., eds., Backbone of the Americas—Shallow subduction, plateau uplift, and ridge and terrane collision: Geological Society of America Memoir 204, p. 85–98. https://doi.org/10.1130/2009.1204(04)

Humphreys, E., Hessler, E., Dueker, K., Farmer, G.L., Erslev, E., and Atwater, T., 2003, How Laramide-age hydration of North America by the Farallon slab controlled subsequent activity in the western U.S.: International Geology Review, v. 45, no. 7, p. 575–595. https://doi.org/10.2747/0020-6814.45.7.575

Irvine, T.N., and Baragar, W.R.A., 1971, A guide to the chemical classification of common volcanic rocks: Canadian Journal of Earth Sciences, v. 8, no. 5, p. 523–548. https://doi.org/10.1139/e71-055

Johnson, D.M., Hooper, P.R., and Conrey, R.M., 1999, XRF analysis of rocks and minerals for major and trace elements on a single low dilution Li-tetraborate fused bead: Advances in X-ray Analysis, v. 41, p. 843–867.

Kelley, V.C., 1971, Geology of the Pecos country, southeastern New Mexico: New Mexico Bureau of Mines and Mineral Resources Memoir 24, 72 p. https://doi.org/10.58799/M-24

Le Bas, M.J., Le Maitre, R.W., Streckeisen, A., and Zanettin, B., 1986, A chemical classification of volcanic rocks based on the total alkali-silica diagram: Journal of Petrology, v. 27, no. 3, p. 745–750. https://doi.org/10.1093/petrology/27.3.745

Le Maitre, R.W., Streckeisen, A., Zanettin, B., Le Bas, M.J., Bonin, B., and Bateman, P., eds., 2002, Igneous Rocks—A classification and glossary of terms: Cambridge, Cambridge University Press, 252 p.

Lepage, L.D., 2003, ILMAT—An Excel worksheet for ilmenite-magnetite geothermometry and geobarometry: Computers & Geosciences, v. 29, no. 5, p. 673–678. https://doi.org/10.1016/S0098-3004(03)00042-6

Li, X., Liu, N., and Zhang, J., 2019, Adsorption of cesium at the external surface of TOT type clay mineral—Effect of the interlayer cation and the hydrated state: Journal of Physical Chemistry C, v. 123, no. 32, p. 19540–19548. https://doi.org/10.1021/acs.jpcc.9b04035

McDonough, W.F., 1990, Constraints on the composition of the continental lithospheric mantle: Earth and Planetary Science Letters, v. 101, no. 1, p. 1–18. https://doi.org/10.1016/0012-821X(90)90119-I

McDonough, W.F., and Sun, S.S., 1995, The composition of the Earth: Chemical Geology, v. 120, no. 3–4, p. 223–253. https://doi.org/10.1016/0009-2541(94)00140-4

McKenzie, D., and O’Nions, R.K., 1991, Partial melt distributions from inversion of rare earth element concentrations: Journal of Petrology, v. 32, no. 5, p 1021–1091. https://doi.org/10.1093/petrology/32.5.1021

McLemore, V.T., 1996, Great Plains margin (alkalic-related) gold deposits in New Mexico, *in* Cyner, A.R., and Fahey, P.L., eds., Geology and ore deposits of the American Cordillera: Geological Society of Nevada Symposium Proceedings, Reno/Sparks, Nevada, April 1995, p. 935–950.

Menzies, M.A., and Murthy, V.R., 1980, Mantle metasomatism as a precursor to the genesis of alkaline magmas—Isotopic evidence: American Journal of Science, v. 280A, p. 622–638.

Mutschler, F.E., Griffin, M.E., Stevens, D.S., and Shannon, S.S., Jr., 1985, Precious metal deposits related to alkaline rocks in the North American Cordillera—An interpretive review: Transactions Geological Society of South America, v. 88, p. 355–377.

Mutschler, F.E., Mooney, T.C., and Johnson, D.C., 1991, Precious metal deposits related to alkaline igneous rocks—A space-time trip through the Cordillera: Mining Engineering, v. 43, p. 304–309.

Mysen, B.O., and Holloway, J.R., 1977, Experimental determination of rare earth fractionation patterns in partial melts from peridotite in the upper mantle: Earth and Planetary Science Letters, v. 34, no. 2, p. 231–237. https://doi.org/10.1016/0012-821X(77)90007-3

New Mexico Bureau of Geology and Mineral Resources (NMBGMR), 2003, Geologic map of New Mexico, scale 1:500,000, 2 sheets. https://doi.org/10.58799/116894

Othman, D.B., White, W.M., and Patchett, J., 1989, The geochemistry of marine sediments, island arc magma genesis, and crust-mantle recycling: Earth and Planetary Science Letters, v. 94, no. 1–2, p. 1–21. https://doi.org/10.1016/0012-821X(89)90079-4

Pearce, J.A., and Norry, M.J., 1979, Petrogenetic implications of Ti, Zr, Y, and Nb variations in volcanic rocks: Contributions to Mineralogy and Petrology, v. 69, no. 1, p. 33–47. https://doi.org/10.1007/BF00375192

Perkins, D., and Anthony, E.Y., 2011, The evolution of spinel lherzolite xenoliths and the nature of the mantle at Kilbourne Hole, New Mexico: Contributions to Mineralogy and Petrology, v. 162, no. 6, p. 1139–1157. https://doi.org/10.1007/s00410-011-0644-1

Ragland, P.C., 1989, Basic Analytical Petrology: New York, Oxford University Press, 369 p.

Ricketts, J.W., Kelley, S.A., Karlstrom, K.E., Schmandt, B., Donahue, M.S., and van Wijk, J., 2016, Synchronous opening of the Rio Grande rift along its entire length at 25–10 Ma supported by apatite (U-Th)/He and fission-track thermochronology, and evaluation of possible driving mechanisms: Geological Society of America Bulletin, v. 128, no. 3–4, p. 397–424. https://doi.org/10.1130/B31223.1

Roden, M.F., 1987, Rb/Sr and Sm/Nd ratios of metasomatized mantle—Implications for the role of metasomatized mantle in the petrogenesis of Na_2O-rich alkaline basalts, *in* Morris, E.M., and Pasteris, J.D., eds., Mantle metasomatism and alkaline magmatism: Geological Society of America Special Paper 215, p. 127–138. https://doi.org/10.1130/SPE215-p127

Rollinson, H., and Pease, V., 2021, Using Geochemical Data: Cambridge, Cambridge University Press, 349 p. https://doi.org/10.1017/9781108777834

Satsukawa, T., Michibayashi, K., Anthony, E.Y., Stern, R.J., Gao, S.S., and Liu, K.H., 2011, Seismic anisotropy of the uppermost mantle beneath the Rio Grande rift—Evidence from Kilbourne Hole peridotite xenoliths, New Mexico: Earth and Planetary Science Letters, v. 311, no. 1–2, p. 172–181. https://doi.org/10.1016/j.epsl.2011.09.013

Semmes, D.R., 1920, Notes on the Tertiary intrusives of the lower Pecos Valley, New Mexico: American Journal of Science, ser. 4, v. 50, p. 415–430.

Shaw, D.M., 2006, Trace Elements in Magmas: Cambridge, Cambridge University Press, 243 p.

Sun, S.S., and McDonough, W.F., 1989, Chemical and isotopic systematics of oceanic basalts—Implications for mantle composition and processes, *in* Saunders, A.D., and Norry, M.J., eds., Magmatism in the ocean basins: Geological Society Special Publication 42, p. 313–345.

Takahashi, E., Shimazaki, T., Tsuzaki, Y., and Yoshida, H., 1993, Melting study of a peridotite KLB-1 to 6.5 GPa, and the origin of basaltic magmas: Philosophical Transactions of the Royal Society of London A, v. 342, no. 1663, p. 105–120. https://doi.org/10.1098/rsta.1993.0008

Woolley, A.R., 1987, Alkaline Rocks and Carbonatites of the World, Part 1—North and South America: University of Texas Press, Austin.

Wyllie, P.J., 1981, Plate tectonics and magma genesis: Geologische Rundschau, v. 70, p. 128–153. https://doi.org/10.1007/BF01764318